



ELSEVIER

Contents lists available at ScienceDirect

Global and Planetary Change

journal homepage: www.elsevier.com/locate/gloplacha

Research paper

Eccentricity-induced expansions of Brazilian coastal upwelling zones

Douglas V.O. Lessa^a, Thiago P. Santos^a, Igor M. Venancio^b, Ana Claudia A. Santarosa^c,
Edmundo C. dos Santos Junior^c, Felipe A.L. Toledo^c, Karen B. Costa^c, Ana Luiza S. Albuquerque^{a,*}^a Programa de Pós-Graduação em Geoquímica, Universidade Federal Fluminense, Niterói 24.020-141, Brazil^b Center for Weather Forecasting and Climate Studies (CPTEC), National Institute for Space Research (INPE), Rodovia Pres. Dutra, km 39, 12.630-000, Cachoeira Paulista, SP, Brazil^c South Atlantic Paleoceanography Laboratory, Oceanographic Institute, University of São Paulo, 05508-120 São Paulo, Brazil

ARTICLE INFO

Keywords:

Southwest Atlantic Ocean
Planktonic foraminifera
Pleistocene
Milankovitch cycles
Paleoceanography

ABSTRACT

Expansions of coastal upwelling spots along the Brazilian coast were previously reported for Marine Isotope Stage (MIS) 5, but open questions remain regarding the climatic mechanisms and the periodicity of such changes. Based on two marine sediment cores, we provide evidence for multiple intensifications of the upwelling regime off the Southeast Brazilian margin (SBM) during several interglacials and highlight the major role of eccentricity as the responsible forcing. In addition, we show a two-step change in the upwelling regime across the Mid-Brunhes Event (MBE) and an increase in the amplitude of upwelling variability after this climatic transition. Our findings point to substantial modifications of the upwelling regions during several glacial-interglacial transitions that probably altered the regional marine productivity regime and the carbon budget.

1. Introduction

The world's largest oceanic upwelling systems are located on the eastern margins of the Pacific and Atlantic Oceans, and several studies have revealed that these upwelling areas were stronger during glacial stages due to intensification of the trade winds (Weber et al., 1995; Kim et al., 2003; Romero and Schmieder, 2006; Matsuzaki et al., 2011). However, western oceanic margins can also host upwelling systems that are relevant to regional productivity, like those in the Cariaco Basin and Arabian Sea (Muller-Karger et al., 2001; Peeters et al., 2002). Similarly, western-boundary upwelling zones are also present along the Southeast Brazilian Margin (SBM). The upwelling in this region results from interactions between the NE wind stress curl along the continental shelf, the instability of the Brazil Current (BC) flow and the sharp modification in the coast line margin, which changes from a N-S to E-W orientation (Rodrigues and Lorenzetti, 2001; Campos et al., 2000; Calado et al., 2010; Belem et al., 2013). These features converge to pump tongues of cold and nutrient-rich South Atlantic Central Water (SACW) towards the surface, enhancing the primary productivity. The geographical distribution of the Brazilian upwelling zones ranges from between 20° S and 28° S, and it includes several small areas along the shelf; within these areas, the Cabo Frio Upwelling System (CFUS, 22° S – 23° S) is the most prominent example, showing a high biological

productivity that encompasses the neritic realm (Valentin, 1984; Albuquerque et al., 2014; Venancio et al., 2014).

Presently (and throughout the Holocene) the occurrence and variability of the CFUS is limited to the coast, continental shelf and the shelf break (Campos et al., 2000; Castelao and Barth, 2006; Souto et al., 2011; Belem et al., 2013; Lessa et al., 2016). However, Portilho-Ramos et al. (2015) indicated that an offshore expansion of the upwelling at 20° S occurred between 110 and 88 ka. Using the relative abundances of the planktonic foraminifera species *Globigerina bulloides* (an indicator of upwelling intensity; Thiede, 1975) in two sediment cores (GL-74 and GL-75) recovered from the upper continental slope, the authors identified abundances of approximately 30% of this species during Marine Isotope Stage (MIS) 5d and 5c (110–90 kyr), an abundance that is currently only present in the CFUS (Lessa et al., 2014). The available data led the authors to suggest that the strong upwelling during this interval resulted from the lower sea-level stand and stronger interaction between the BC and the Abrolhos Bank, which increased the instability in the BC flow. Applying a similar approach in a near-continental slope core (GL-1090), Lessa et al. (2017) found abundances of *G. bulloides* as high as 25% during the high sea-level stand of the Last Interglacial (MIS 5e), contradicting the possibility that sea-level fluctuations influenced the upwelling process. Based on these observations, the authors proposed the alternative explanation that variations in Earth's orbit, which

* Corresponding author at: Programa de Geoquímica Ambiental, Universidade Federal Fluminense, Outeiro São João Baptista s/n., Niterói 24.020-141, Rio de Janeiro, Brazil.

E-mail address: ana_albuquerque@id.uff.br (A.L.S. Albuquerque).

<https://doi.org/10.1016/j.gloplacha.2019.05.002>

Received 22 October 2018; Received in revised form 28 April 2019; Accepted 2 May 2019

Available online 03 May 2019

0921-8181/ © 2019 Elsevier B.V. All rights reserved.

are governed by eccentricity and cause modulations in seasonality, were the major driving force for the expansion of the CFUS conditions beyond the shelf break. Strong seasonality led to warmer-than-present summers and enhanced NE winds that boosted the upwelling of SACW during the Last Interglacial (Lessa et al., 2017). Although previous studies proposed different mechanisms, it is unambiguous that the CFUS presented an expanded mode that probably carried its high-carbon accumulation zone to offshore regions.

Nevertheless, a consensus regarding the main forcing that modulates the long-term variability of the CFUS has not yet been reached. To investigate the validity of the orbitally-induced mechanism, i.e., the variations in Earth's eccentricity, additional data are needed that cover several interglacial periods, especially the so-called super-interglacial MIS 11 (Droxler et al., 2003), which had the most similar orbital features to those of the Holocene in the past 500 ka (Berger, 1978; Candy et al., 2014). If the mechanism described by Lessa et al. (2017) is correct, then a Holocene-like pattern should be seen in the SBM during MIS 11. Here, we present new data from two sediment cores that together record the last 772 ka, thus covering the last eight interglacial periods (MIS 1–19). Despite some exceptions, planktonic foraminifera indicator species and time-series analyses strongly indicate that the main mechanism shaping the long time-scale pattern of the CFUS conditions is indeed modifications in the eccentricity parameter (100-ka periodicity). Furthermore, we demonstrate that the South Atlantic circulation rearrangement during the Mid-Brunhes Event (MBE), a global climate transition that increased the amplitude of the glacial-interglacial cycles (Berger and Wefer, 2003), moved the thresholds of the CFUS conditions and led to larger upwelling fluctuations after 400 ka. Our data confirm that, opposite to the pattern depicted for eastern margin systems, the wind-driven upwelling in the western margin of the South Atlantic was driven by equatorial-sourced winds that increased during interglacial conditions.

2. Regional settings

The SBM (20–28° S), which encompasses the Campos (20–23° S) and Santos (23–28° S) basins, is shown in Fig. 1. In this region, the surface layer (0–200 m) is characterized by warm and oligotrophic Tropical Water (TW), with temperatures between 18 and 27 °C and salinity above 36 (Silveira et al., 2000). The presence of the TW in the photic zone of the BC limits productivity in this area. The South Atlantic Central Water (SACW), formed in the Brazil-Malvinas Confluence zone at 38° S (in the vicinity of the mouth of the River Plata), flows in the thermocline layer. The SACW sinks and flows beneath the TW in the Subtropical Front at 200–800 m, recirculates in the Subtropical Gyre, and is then incorporated into the BC at about 20° S (Stramma and England, 1999). The SACW has a temperature range of 6–18 °C and a salinity range of 34.5–36 (Silveira et al., 2000). The SACW is the water mass responsible for the high productivity events in the SBM, where it upwells into the photic zone.

Despite the predominant oligotrophic scenario in the subtropical western South Atlantic, some important shelf upwelling zones occur along the SE Brazilian continental shelf, including: (1) the Vitória Upwelling System at 20° S generated via the cyclonic Vitória Eddy that is formed by friction between the BC and Abrolhos Bank (Schmid et al., 1995; Gaeta et al., 1999; Arruda et al., 2013); (2) the Cabo de São Tomé (Calado et al., 2010); (3) the Cabo Frio Upwelling System (CFUS) between 22°–23° S, which is the most important upwelling zone, presenting a high biological productivity zone encompassing the neritic realm (Valentin, 1984; Albuquerque et al., 2014; Venancio et al., 2014); and, (4) the Cabo de Santa Marta Upwelling System at 28° S. These upwelling systems are induced by the topography of the continental margin and interactions with the tropical-sourced NE winds that promote BC instability and wind stress curl along the continental shelf. These features induce SACW upwelling either on the coast and shelf or on the shelf break (Campos et al., 2000; Castela and Barth, 2006;

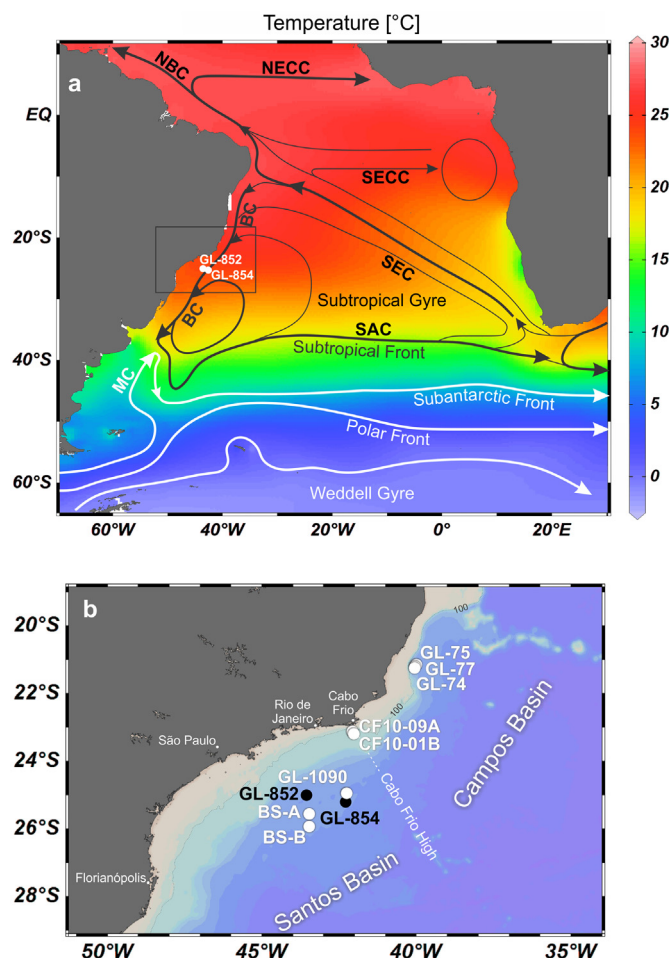


Fig. 1. (a) Map of the South Atlantic surface circulation (modified from Peterson and Stramma, 1991) showing the spatial distribution of sea surface temperature and the locations of the studied cores (GL-852 and GL-854). (b) View of the study area (black rectangle in (a)) showing the bathymetry (filling), the 100-m isobath, the location of the GL-852 and GL-854 cores (this study, black circles) and the cores from the Santos (24° S) and Campos (21° S) basins used for comparison (Portilho-Ramos et al., 2015; Petro et al., 2016; Lessa et al., 2014; Lessa et al., 2016; Lessa et al., 2017; Almeida et al., 2015). Acronyms: SEC – South Equatorial Current; SECC – South Equatorial Countercurrent; NBC – North Brazil Current; NECC – North Equatorial Countercurrent; BC – Brazil Current; SAC – South Atlantic Current; MC – Malvinas (Falkland) Current.

Campos et al., 2013; Belem et al., 2013; Aguiar et al., 2014).

The CFUS is located on the continental shelf near the locations of our cores (GL-852 and GL-854) and can, therefore, be used as a control area to evaluate variations in upwelling in relation to our reconstructions using planktonic foraminifera assemblages. In areas adjacent to the CFUS, the relative *G. bulloides* abundance remained below 5% throughout the Holocene and the last deglacial (Toledo et al., 2008; Lessa et al., 2014; Portilho-Ramos et al., 2015). However, within the CFUS, the relative abundance of *G. bulloides* during the Holocene reached $18 \pm 5\%$ for specimens $> 150 \mu\text{m}$ (Lessa et al., 2014; Lessa et al., 2016). Similar relative abundance values were also observed in important eastern-boundary upwelling systems (Giraudeau et al., 1993; Kucera et al., 2005; Mohtadi et al., 2005, 2007).

3. Materials and methods

The sediment cores GL-852 (25°01'S, 43°33'W, 1938 m, 20.30 m core length) and GL-854 (25°12'S, 42°37' W, 2220 m depth, 20.38 m core length) were collected by Petrobras on the Santos Basin

continental slope in the Santos Drift, southeastern Brazilian Continental Margin, during the Fugro Explorer Campaign 2007 (Fig. 1). GL-852 covers the last 321 kyr and has a mean sedimentation rate of ca. 7.4 cm/kyr, while GL-854 covers the last 772 kyr with a mean sedimentation rate of 4 cm/kyr. Age models of both cores were based on benthic foraminifera $\delta^{18}\text{O}$ stratigraphy and supported by three radiocarbon AMS dates on top of the core GL-854. Detailed descriptions of the age modeling of cores GL-852 and GL-854 age modeling are provided by Almeida et al. (2015) and Toledo et al. (2016).

Samples for planktonic foraminifera analyses were dry-sieved in a 150 μm mesh and then split into subsamples containing at least 300 foraminifera specimens (95% confidence level for species of 1% abundance, Patterson and Fishbein, 1989; Al-Sabouni et al., 2007). These subsamples were stored in micropaleontological slides, identified and counted. Identification followed the taxonomic criteria of Bolli and Saunders (1985) and Hemleben et al. (1989). Planktonic foraminifera assemblages were analyzed with a 5-cm resolution for core GL-854, and for GL-852, 10 cm intervals were used between the core top and 1040 cm and 5 cm intervals were used from 1045 cm to the base of the core. A total of 406 samples were analyzed for GL-854 with a temporal resolution of ca. 2 kyr, and a total of 300 samples were analyzed for GL-852 with a temporal resolution varying from 0.5 to 1 kyr. Using census counts of planktonic foraminifera, we calculated the relative abundances of *Globigerinoides ruber* and *G. bulloides*. The white *G. ruber* morphotype is dominant in the BC, inhabits the surface mixed layer and tends to be more abundant during the austral summer, indicating the occurrence of warm waters (Venancio et al., 2016; Venancio et al., 2017), whereas *G. bulloides* is restricted to the CFUS whose upwelling frequency is also higher during the austral summer due to wind regime, indicating the occurrence of upwelling events when the percentages are above 10% (Lessa et al., 2014). The count of the *G. bulloides* specimens also included *Globigerina bermudezi* specimens since the only difference between the taxa is an anomalous last chamber in *G. bermudezi*. We estimated the paleotemperatures at a depth of 100 m by applying the Modern Analog Technique (MAT) (Hutson, 1980). To calculate MAT-derived temperature at 100 m (MAT_{100m}), we used the MARGO project databank of 891 core tops with planktonic foraminifera assemblages and temperature values from the entire Atlantic (Kucera et al., 2005). In addition, another 161 core tops from upwelling areas off Iberian Peninsula and NW Africa (Salgueiro et al., 2008) were added to the databank to include analogs for upwelling conditions. We maintained the same modeling criteria as Lessa et al. (2017) for GL-852 and GL-854 paleotemperature reconstructions. The MAT-based reconstruction of the temperature model at 100 m had a coefficient of determination (R^2) of 0.98 and a root-mean-square error of prediction (RMSEP) of 0.864 °C. Graphical and numeric representations of the model performances are shown in the supplementary material.

To verify the presence of periodicity in the data from the GL-852 and GL-854 cores, we performed time-series analysis. The REDFIT analysis (Schulz and Mudelsee, 2002) was used with the software PAST (Hammer et al., 2001). For analyzing the data with this approach, we chose the Welch-type spectral window, setting the oversample to 4 and the segments to 2. In addition, we performed a wavelet analysis, based on the Morlet wavelet, using the same software. The data were interpolated using the nearest neighbor value prior to the analysis.

4. Results

High levels of *G. ruber* occurred before 640 kyr and during the last five glacial periods (MIS 12 to 2) (Fig. 2A). The highest values for *G. ruber* relative abundance (> 60%) occurred in short episodes during MIS 7, 5 and 3, and the lowest values occurred during MIS 13 and in short episodes during MIS 9 and 8. The relative abundances of *G. bulloides* ranged from 0 to 27% in both cores (averages of 9.1% and 7.6% in cores GL-854 and GL-852, respectively) (Fig. 2B). The highest levels of *G. bulloides* occurred, in general, during terminations and during the

onset of interglacial periods. Furthermore, the values were usually above 10% before 470 kyr (MIS 12) and then later decreased to < 10%, while maintaining peaks of very high values (> 15%) during MIS 9, 7 and 5, and low values during MIS 11, 10, 8, 6, 4, 2 and 1. The relative abundance of *G. ruber* ranged from 9 to 74% (averages of 37% and 39% in cores GL-854 and GL-852, respectively) (Fig. 2a). The *G. bulloides* to *G. ruber* ratio (Gb/Gr) shows that during MIS 13 and MIS 9 the relative abundance of *G. bulloides* was similar or even higher than that of *G. ruber*, which is not observed under modern conditions (Fig. 2c). The MAT_{100m} reconstruction for GL-854 showed values below 18 °C before 425 kyr and generally high values (> 18 °C) from 217 kyr to the present. Variations in the MAT_{100m} values from both cores are very similar over the last 321 kyr (Fig. 2d). Spectral analysis revealed the presence of a strong 100-kyr periodicity in the relative abundance of *G. bulloides* (Fig. 4a) and a 23-kyr periodicity in the relative abundance of *G. ruber* in core GL-854 (Fig. S2B), and both periodicities were above a 99% confidence level. Spectral analysis of the relative abundance of *G. bulloides* in core GL-854 also revealed the presence of cycles of ca. 8–11 kyr above the 95% confidence level (11-kyr cycle was even above 99% confidence level). Wavelet analysis also indicated that the 100-kyr periodicity in the relative abundance of *G. bulloides* is significant over the entire record (Fig. 4b). Statistically significant periodicities ranging between 8 and 11 kyr were also revealed by the Wavelet analysis but were not constantly present in the record. Other cycles were identified in our dataset, but they presented low power and/or were only significant at a 95% confidence level (see supplementary material).

5. Discussion

5.1. Rhythmic expansion and retraction of the SE Brazilian upwelling system

Currently, the strength of the NE winds that blow stronger during the austral summer is a crucial factor driving the continental shelf upwelling in the SBM (Valentin et al., 1987). Consequently, past periods of intensified summer-like conditions probably favored upwelling episodes in this area. A set of cores collected on the upper continental slope shows a high relative abundance of the upwelling-indicator species *G. bulloides* (exceeding 20%) and a shoaling of the 18 °C isotherm during MIS 5 (Lessa et al., 2017). Lessa et al. (2017) concluded that the high eccentricity during MIS 5 increased regional seasonality, consequently strengthening the NE winds, which ultimately led to the strong upwelling episodes that occurred beyond the continental shelf. We compared the relative abundance of *G. bulloides* in cores GL-852 and GL-854 to the framework built by Lessa et al. (2017) for MIS 5 (Fig. 3). The new data from both records agree fairly well with the previously proposed concept, i.e., a larger occurrence of *G. bulloides* coevals with high eccentricity in Earth's orbit. When the eccentricity values decreased substantially near the end of MIS 5, all six records registered relative abundances of *G. bulloides* below 10% (Fig. 3). This good agreement makes GL-852 and GL-854 suitable for addressing the variability of the upwelling system on longer time-scales. However, there are still two conditions that must be satisfied to confirm the role of eccentricity over the expansion and retraction of the upwelling system. The first condition is the identification of the 100-ka main signal associated with eccentricity in these new long records. The second condition is related to the upwelling variability around MIS 11. Despite being one of the longest interglacial periods of the Quaternary (Yin and Berger, 2015) that could boost upwelling at the Brazilian coast, MIS 11 shared similar orbital configurations with MIS 1 (Desprat et al., 2007); therefore, it should present a retracted upwelling configuration like that of MIS 1 (Lessa et al., 2017).

To verify the presence of eccentricity modulation in our data, we performed time series analysis with *G. bulloides* relative abundance in the core GL-854. The spectral analysis results for core GL-854 show a prominent 100-ka peak that presents the highest spectral power and is

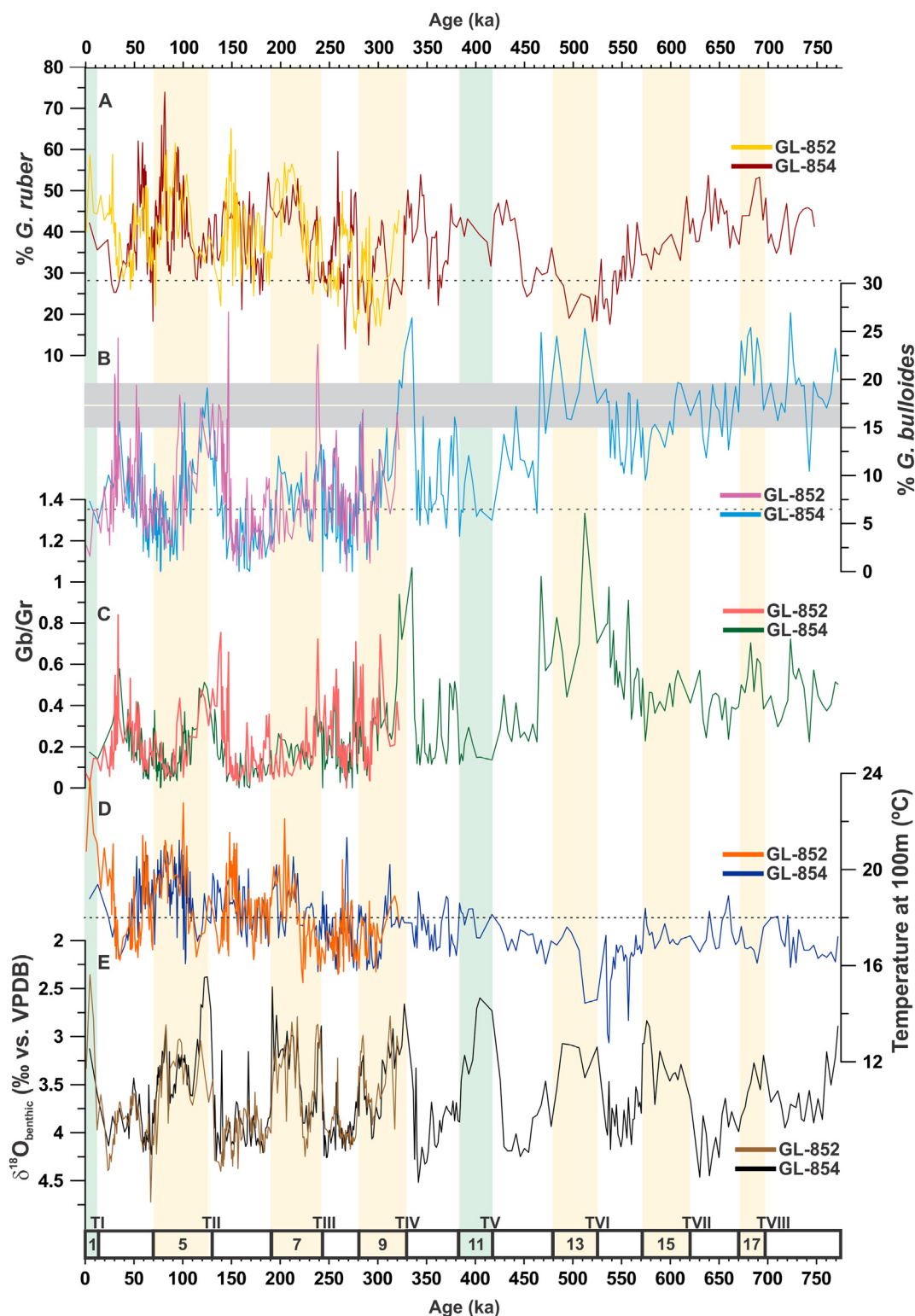


Fig. 2. Results of cores GL-852 and GL-854. A: Relative abundance of *Globigerinoides ruber*. B: Relative abundance of *Globigerina bulloides*. The continuous line, grey filling and dashed lines represent CFUS average, standard deviation and extreme values, respectively, during the Holocene (Lessa et al., 2014, 2016). C: Ratio between *G. bulloides* and *G. ruber* (Gb/Gr). Temperature (°C) derived from the Modern Analogue Technique (MAT) at 100 m. The dashed line highlights the 18 °C isotherm in reference to the recent SACW/TW boundary. E: Oxygen isotope composition of *Cibicides wuellerstorfi* used to develop the age models of both cores (Toledo et al., 2016). The yellow bars highlight the warm Marine Isotope Stages of the last ca. 750 ka. The green bar highlights the Marine Isotope Stage 1 and 11. (For interpretation of the references to colour in this figure legend, the reader is referred to the web version of this article.)

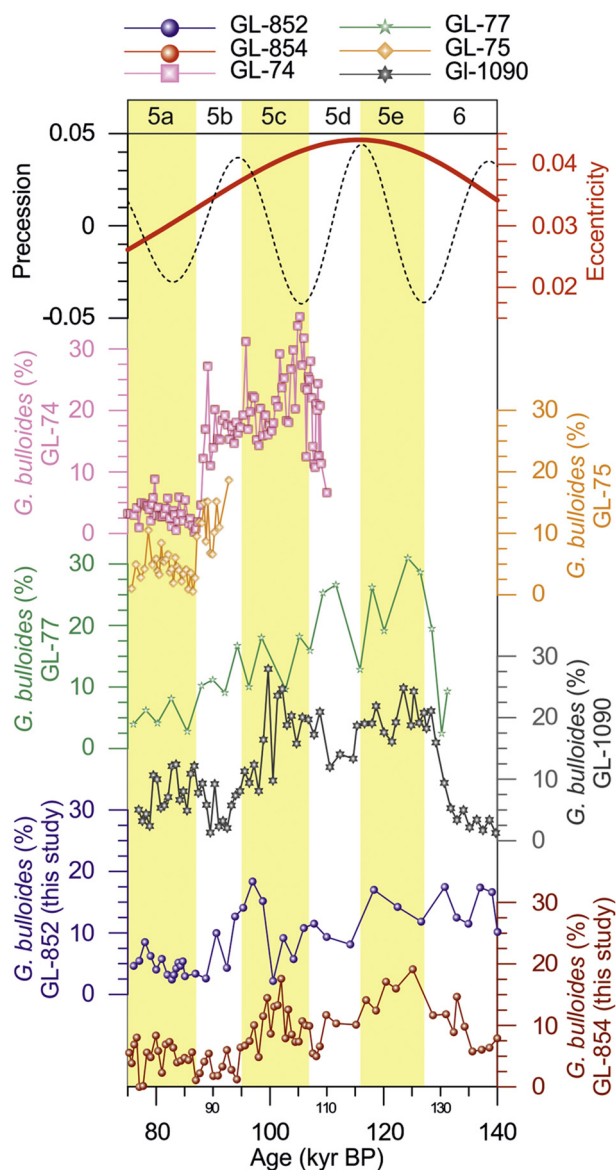


Fig. 3. Comparison of orbital parameters (extracted from Berger and Loutre, 1991) and relative abundance of *G. bulloides* in cores GL-852 and GL-854 (this study), GL-74 and GL-75 (Portilho-Ramos et al., 2015), GL-77 (Petro et al., 2016) and GL-1090 (Lessa et al., 2017). Values between 15 and 19% are similar to values observed in the Cabo Frio Upwelling System during the Holocene (Lessa et al., 2014, 2016). The yellow bars mark the warm substages of Marine Isotope Stage 5. (For interpretation of the references to colour in this figure legend, the reader is referred to the web version of this article.)

significant at over a 99% confidence level (Fig. 4a). Wavelet analysis indicates that such a 100-ka periodicity is present over the entire time series and that it is not related to a specific interval in GL-854 (Fig. 4b). Furthermore, the 100-ka cycle is also present in the MAT_{100m} dataset (see supplementary material), which reinforces the conclusion that the increase in the relative abundance of *G. bulloides* resulted from a shoaling of the 18 °C isotherm induced by enhanced summer NE winds. These analyses show that eccentricity was indeed the dominant forcing over the entire record that modulated the upwelling changes off the Brazilian coast (Fig. 4). Eccentricity values as high as 0.033 seem to trigger SBM upwelling expansion, as reported by Lessa et al. (2017). The eccentricities during MIS 19, 17, 13, 9, 7 and 5 reached values above this threshold, with the maximum values lying very close to or above 0.04 in most cases. Consequently, such high eccentricities may have influenced the wind regime by controlling precession cycles and,

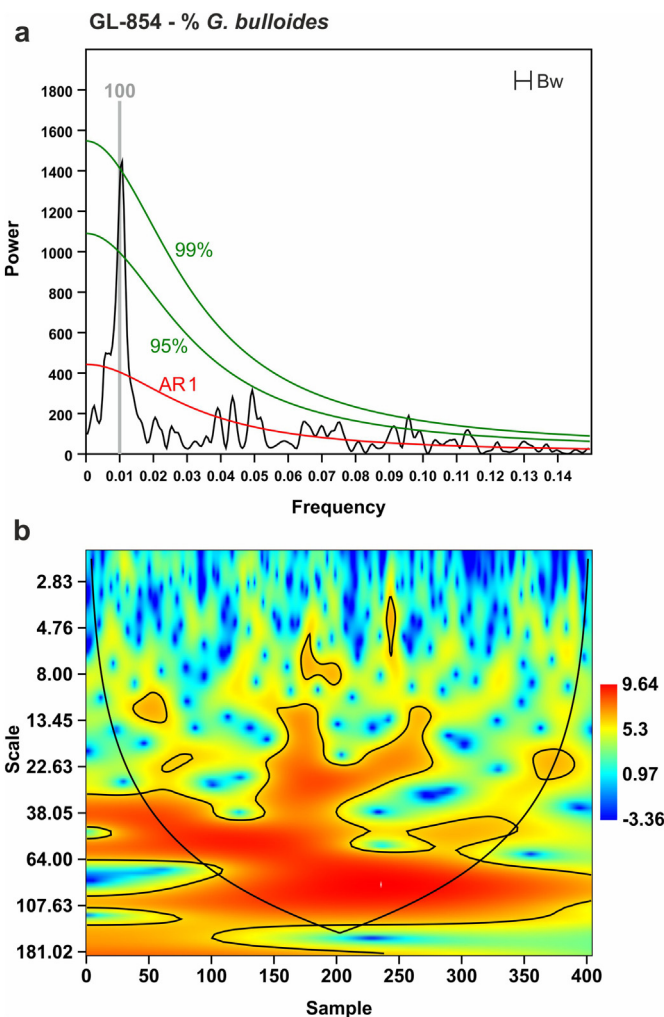


Fig. 4. Time series analyses of the relative abundances of *G. bulloides* in core GL-854. (a) Spectral analyses performed with the REDFIT algorithm (Schulz and Mudelsee, 2002) and the PAST software (Hammer et al., 2001). The red line represents the red-noise spectrum and the green lines show the 95 and 99% confidence levels. The black symbol indicates the 6-dB bandwidth (Bw) related to the frequency resolution. The grey bar highlights the 100-kyr periodicity. (b) Wavelet analysis performed in the same software. Signal power is shown with a colour scale. (For interpretation of the references to colour in this figure legend, the reader is referred to the web version of this article.)

consequently, the intensity of the insolation during the seasons, especially during the summer when the NE winds are more intense, thus favoring offshore expansion. On the other hand, the estimated eccentricity for MIS 11 is below 0.02 (similar to that of MIS 1), and this value would not be favorable for promoting expansion of the upwelling system.

In general, the relative abundance of *G. bulloides* exceeds 20% in cores GL-852 and GL-854, either at the maximum or approaching the high eccentricity periods during MIS 5, 7, 9, 13 and 17. Exceptions to this pattern occurred in an interval during the last glacial (early- to mid-MIS 3), when an exceptionally high relative abundance was coincident with low eccentricity, and during MIS 15, when a smaller *G. bulloides* peak occurred at a time of very high eccentricity. Despite these deviations from the pattern proposed here, time-series analysis of the relative abundances of *G. bulloides* in core GL-854 supports the 100-ka periodicity that is present over the entire time series and that is not related to a specific interval in GL-854 (Fig. 4b). These analyses show that eccentricity is the dominant forcing throughout the entire record (Fig. 4), confirming the relevance of this climatic forcing in driving the

upwelling changes off the Brazilian coast.

A second significant harmonic signal, albeit with considerably smaller spectrum power, is a ca. 10.5 ka periodicity that could be related to semi-precessional variability. Berger et al. (2006) showed that the double maximum that characterizes the daily radiation received in tropical latitudes over the course of the year explains why equatorial insolation presents harmonic signals related to the eccentricity (123 and 95 ka) and semi-precession (11 and 5.5 ka) cycles. According to these authors, the amplitude of such signals rapidly decreases moving away from the equator, where, for example, at 5°N, the eccentricity prevalence is already supplanted by precession. Modeling experiments also demonstrate that in equatorial areas, a temperature signal with significant amplitude is predicted in the eccentricity and semi-precession bands and can be directly explained by a nonlinear response to the local insolation (e.g., Laepple and Lohmann, 2009). Based on the results from Laepple and Lohmann (2009), the subtropical region where GL-854 was collected would be more prone to modulation by precession. However, significant periodicities associated with eccentricity and semi-precession were observed in the relative abundance of *G. bulloides*, suggesting the existence of an equatorial-like mode of variability that can modulate upwelling expression at latitudes as far south as 24°S in the western South Atlantic.

The NE winds that blow parallel to the SE Brazilian coast and favor the occurrence of *G. bulloides* represent the western border of the South Atlantic high-pressure system (SAH) (Garreaud et al., 2009). Today, this anticyclonic system is largest and strongest during the solstitial months, and during the austral summer, its center is located farthest from the equator with more frequent westward than eastward excursions (Sun et al., 2017). The consequence of a south and west displacement of the SAH is an expansion of the NE winds field along the SBM (Reboita et al., 2019), which may lead to warmer and drier summers in our study site (Silva et al., 2015; Coelho et al., 2016). Such a scenario would be prone to the occurrence of increased episodes of persistent of NE winds, which boost the upwelling. Consistently, a model investigation reported a warmer and drier climate over the eastern South American continent during the Last Interglacial (MIS 5e) compared to that of the pre-industrial period (Fischer and Jungclauss, 2010). Such a scenario was also seen in paleoreconstructions based on speleothems in the Brazilian Southeast (Cruz et al., 2006). These authors observed increased suppression of the South American monsoon over precipitation over the region between 130 and 105 kyr BP, which is consistent with the model simulations. Such conditions support the possibility of that the presence of the SAH may have been present more frequently over the South American continent during previous interglacials. Based on these descriptions and our current results, we propose that orbital cycles, of which eccentricity is the most important parameter, have the strongest control over spatial and temporal variations in NE wind episodes. High relative abundances of *G. bulloides* occurred in phase with reversed precession phases, suggesting that long-term NE winds episodes would be favored during aphelian austral summers. Aphelian summers are less intense but longer compared to the more intense and shorter, perihelian summers (Kostadinov and Gilb, 2014). Therefore, aphelian summers could be responsible by maxima of relative abundances of *G. bulloides* during both glacial and interglacial periods. Despite the observed relationship between *G. bulloides* relative abundance and reversed precession, Fig. 5 shows that both the amplitude and timing of abundance peaks varied throughout the record. Thus, caution should be taken when considering a direct link between upwelling expansion and a reversed phase of precession over the entire record.

The 100-ka periodicity is not the sole harmonic associated with eccentricity variance. Long-term variations in Earth's orbit are superimposed on a longer cycle of about 400-ka, although this cycle is essentially absent in the frequency spectrum of the ice volume variations (Berger et al., 2007; Ganopolski and Calov, 2011). We did not expect the 400-ka periodicity to appear in the spectral analysis of GL-854 due

to the length of the time series. However, the long-term modulation of the 400-ka cycle results in some interglacial periods of damped eccentricity amplitude, which over the last one million years are exemplified by MIS 1, 11 and 19. The relative abundances of *G. bulloides* in core GL-854 during MIS 11 shows values that barely exceed 10%, suggesting a retreat of the upwelling system to the continental shelf, which is quite different from earlier and later interglacial periods. The variability in the *G. bulloides* abundance during MIS 11 was, in fact, considerably similar to that of MIS 1. Because MIS 1 and 11 had comparable orbital configurations (Müller and Pross, 2007), this result was expected in light of the eccentricity-induced upwelling mechanism previously proposed by Lessa et al. (2017). Therefore, in general, the observed changes (expansion or retraction) in the Brazilian coastal upwelling system can be attributed to variations in Earth's orbit.

5.2. Upwelling variability across the Mid-Brunhes Event

In addition to demonstrating that eccentricity controls the variability of the SE Brazilian coastal upwelling expansion and retraction on long time-scales (Fig. 5b), the new data obtained from GL-854 and GL-852 show dynamic ocean circulation changes around 430 ka that can be linked to the Mid-Brunhes Event (MBE). The MBE was the most pronounced climatic shift during the last 800 ka and represents a step-like change in the intensity of interglacial warmth that occurred between MIS 13 and 11 (PAGES, 2016). Antarctic ice-cores show an increase in temperature and $p\text{CO}_2$ after the MBE (Fig. 5d), which support a broad global impact of this shift (Epica, 2004); however, its geographical coverage as a global event is controversial (Meckler et al., 2012). Recent reconstructions of CO_2 concentrations based on planktonic foraminifera $\delta^{11}\text{B}$ revealed that the interglacials prior to MIS 19 had CO_2 concentrations similar to those observed in MIS 11 and that the cooler temperatures during MIS 19 to MIS 13 were due to a transition linked to the restructuring of the 100 kyr cycles (Chalk et al., 2017). According to Candy and McClymont (2013), in any record including the MBE, the so-called “MBE intensity” will always have values above zero. We applied their methodology but adapted it to our case by considering only the glacial-interglacial variability in *G. bulloides* abundance during high eccentricity periods, i.e., MIS 17, 15 and 13 (pre-MBE) and MIS 9, 7 and 5 (post-MBE). Based on this analysis, we estimated an MBE intensity of 9.24 and, therefore, provide support to an unequivocal connection between this climate transition and the Brazilian upwelling system.

Even though the eccentricity imprint was observed prior to the MBE, the background percentages of *G. bulloides* were constantly above 10%. > 15% of the background in *G. bulloides* relative abundance occurred prior to MIS 16 (Fig. 5c), and the $\text{MAT}_{100\text{m}}$ was usually lower than 18 °C prior to MIS 11 (Fig. 2d). These data suggest that the SBM maintained high productivity conditions prior to MIS 11. However, information about pre-MBE South Atlantic Ocean surface circulation is scarce, and previous studies reported that the Subtropical, Subantarctic and Polar fronts were displaced northward (Becquey and Gersonde, 2002). In addition, Barth et al. (2018) reported high negative $\delta^{13}\text{C}$ anomalies associated with intensified wind driven Antarctic upwelling prior to MBE, with a maximum occurring between MIS 14 and 13. Based on these observations, these authors suggested that the Antarctic Bottom Water (AABW) could have expanded northwards, impacting not only its physico-chemical properties such as geometry and ventilation, but also the deep ocean carbon reservoir. Even though the $\delta^{13}\text{C}$ stack of Barth et al. (2018) demonstrated changes in properties of the AABW, we cannot discard the possibility that such effects, driven by the wind-driven Antarctic upwelling, also affected the physico-chemical properties of the Antarctic intermediate and mode waters. The enhanced wind driven Antarctic upwelling mechanism was demonstrated by Yin (2013) to be driven by changes in the Earth's orbital configuration, in especial by low obliquity austral summers. This oceanographic scenario possibly increased the contribution of Antarctic waters and the nutrients present in the SACW (Barth et al., 2018), thus boosting productivity in our

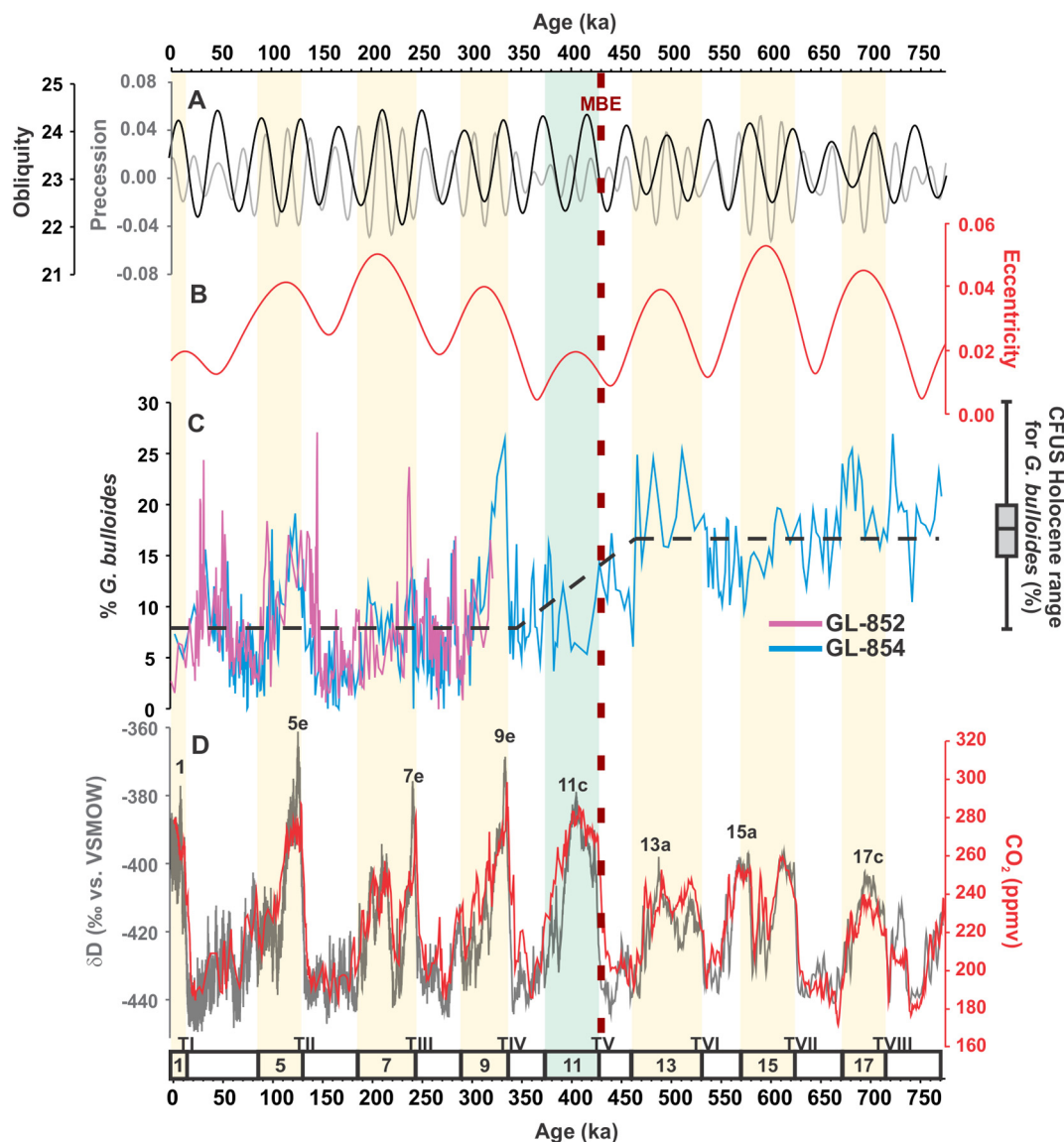


Fig. 5. Two-step change in the relative abundances of *G. bulloides* across the Mid-Brunhes Event. A: Precession (grey line) and obliquity (black line) from Berger and Loutre (1991). B: Eccentricity (red line) from Berger and Loutre (1991). C: Relative abundances of *G. bulloides* from cores GL-852 (purple line) and GL-854 (blue line). D: Antarctic δD (grey line) and CO_2 concentration (red line) from EPICA (2004) plotted on the AICC2012 time-scale (Bazin et al., 2013; Veres et al., 2013). The boxplot shows *G. bulloides* abundance variation in the Cabo Frio Upwelling System (CFUS) during the Holocene, where the solid line and grey box represent recent mean and standard deviation, respectively (Lessa et al., 2014, 2016). (For interpretation of the references to colour in this figure legend, the reader is referred to the web version of this article.)

study area and causing changes in the planktonic community (i.e., increases in productivity-related species like *G. bulloides*). Changes in the planktonic community were also observed by Schmieder et al. (2000) and by Romero and Schmieder (2006) who reported sediment layers composed of the giant diatom *Ethmodiscus rex* in the subtropical South Atlantic, which are rarely found in modern sediments under equatorial upwelling zones. Thus, enhanced SACW nutrient concentrations caused by changes in the pre-MBE South Atlantic may have contributed to our observation of the high *G. bulloides* levels in the SBM during the pre-MBE glacial.

Regarding the climatic transition experienced around the MBE, the upwelling pattern changed in three different ways. The first change was related to the shape of the *G. bulloides* peak during the interglacials. In the post-MBE interglacial periods, most notably MIS 9, 7 and 5, the warmth peak occurred coincident with the first maximum summer insolation in the high northern hemisphere (Berger, 1978). Because of this relationship, the warmest interval encompassed the first warm

substages (MIS 9e, 7e and 5e), thus resulting in a relatively fast, high-magnitude climate amelioration after the end of previous glacial stage (Lisiecki and Raymo, 2005). This outcome was not the case for the pre-MBE interglacial periods, as their peak warmth tended to occur later and more than one climate optimum existed. Because of these features, the pre-MBE interglacial periods, most notably MIS 17 and 13, had more than one peak in *G. bulloides* relative abundance with more uniform values throughout the warm stages. On the other hand, the post-MBE interglacial periods MIS 9, 7 and 5 had unique *G. bulloides* peaks in parallel to the maximum warmth already reached at the beginning of each warm stage. The fact that changes in the variation pattern of *G. bulloides* relative abundance occurred at the MBE supports our interpretation that the upwelling system is strongly linked to the interglacial climate.

In addition to the changes in the shape of the *G. bulloides* peaks, a second feature regarding the mean values of the *G. bulloides* relative abundances should be highlighted. Prior to the MBE, the relative

abundances of *G. bulloides* exhibit a mean value of 16.5%, while the post-MBE mean value is 7.3%. This difference indicates that the pre-MBE oceanographic conditions mentioned above such as cooler waters and varying plankton composition probably favored a larger *G. bulloides* population. Our MAT_{100m}-derived temperature profile indicated strong temperature decreases during MIS 14 and early MIS 13 (Fig. 2d), which comprises the beginning of the MBE, as reported by Barth et al. (2018). Such an episode is described as a pronounced geometry change in the Antarctic waters that promoted an above-mean glacial equatorwards displacement of the Southern Ocean fronts (Becquey and Gersonde, 2002; Yin, 2013). The fact that the Subtropical Gyre's mixed layer was under greater influence of Subantarctic waters (Schmieder et al., 2000), combined with a high productivity-adapted plankton community and intense NE winds during MIS 13, probably favored an increase in the *G. bulloides* population in the subsurface layers (Fig. 5c). This observation suggests that cold and nutrient-rich waters were probably present in the upper ocean during the pre-MBE glacial and interglacial stages. This prediction is supported by our MAT_{100m} data (Fig. 2d), which show values below 18 °C (the uppermost limit of the SACW) for almost the entire pre-MBE phase.

The third and most important modification observed across the MBE were significant changes in the amplitude of *G. bulloides* abundance during glacial-interglacial transitions. Fig. 5c shows that the pre-MBE period (with the exception of MIS 14) was marked by *G. bulloides* abundances of about 15% during the glacials and > 20% during the interglacials. After the MBE, the glacial stages were characterized by a much lower *G. bulloides* abundance of approximately 5%; however, the maximum interglacial peaks still remained above 20%. These differences indicate that the post-MBE glacial periods disrupted the ecological preferences of *G. bulloides* more profoundly than the pre-MBE glacial periods. The unfavorable conditions for *G. bulloides* can also be seen in the MAT_{100m} data, which indicated a gradual deepening of the 18 °C isotherm from the MBE towards the present. The southwards retreat of the AABW and the establishment of the post-MBE properties of the Antarctic water masses made the South Atlantic circulation more prone to produce heat reservoirs below the surface layer during the glacials (e.g. Santos et al., 2017). Therefore, we assume that the glacial heat storage property of the Brazil Current and the loss of the pre-MBE properties of the SACW probably reduced the fertilization of the shallower layers leading to a deeper thermocline and lower *G. bulloides* abundance. These conditions would have favored a prevalence of warm and oligotrophic species, such as *G. ruber*, in the water column (Fig. 2A and B). However, a likely intensification of the NE winds, as previously argued, in parallel to the strengthening of the post-MBE interglacials, could have interrupted the preferential glacial disruption of *G. bulloides* and then increased its abundance to levels as high as those observed during the pre-MBE interglacials (Fig. 5c). Therefore, our data indicate that a strengthening of the SBM upwelling system occurred after the MBE, creating a wider and more productive upwelling zone during times in which the Earth's orbit had higher eccentricity. These results exemplify how planetary-scale phenomena may modulate regional climates.

6. Conclusions

Our data support the occurrence of offshore-expanded SE Brazilian upwelling events during MIS 5 (which have been previously shown by other studies) and show that this pattern was common to other interglacials characterized by high eccentricity. The analogous retreated upwelling conditions during MIS 1 and MIS 11 and the prominent 100-kyr periodicity observed in our data support the role of orbit's eccentricity as the dominant factor contributing to upwelling system expansion. Furthermore, we showed that the expanded upwelling system persisted perennially during the Middle Pleistocene, occasionally expanding across the MBE and Late Pleistocene. These observations reinforce the argument that the MBE was a global climatic transition that

had a major influence on the southwest Atlantic oceanic circulation. Future studies should focus on the consequences of such upwelling expansions for marine productivity and carbon accumulation in oceanic sediments.

Funding

This study was supported by the CAPES-ASPECTO project (grant 88887.091731/2014-01). This study was financed in part by the Coordenação de Aperfeiçoamento de Pessoal de Nível Superior - CAPES/Brazil - Finance Code 001. Douglas V. O. Lessa acknowledges financial support from CAPES (grant PE 99999.000042/2017-00). CAPES currently supports Igor M. Venancio financially with a scholarship (grant 88887.156152/2017-00). A.L.S. Albuquerque is a CNPq (National Council for the Development of Science and Technology, Brazil) senior researcher (grant 302521/2017-8).

We thank R. Kowsman (CENPES/Petrobras) and the Petrobras Core Repository staff (Macaé/Petrobras) for providing the sediment core used in this research. We also thank the two anonymous reviewers for their important contributions to enriching the manuscript.

Data availability

Datasets related to this article will be available at www.pangaea.de after the acceptance of the manuscript. At this time, the data required to reproduce these findings cannot be shared due to ethical reasons as the data also forms part of an ongoing study.

Appendix A. Supplementary data

Supplementary data to this article can be found online at <https://doi.org/10.1016/j.gloplacha.2019.05.002>.

References

- Aguiar, A.L., Cirano, M., Pereira, J., Marta-Almeida, M., 2014. Upwelling processes along a western boundary current in the Abrolhos-Campos region of Brazil. *Cont. Shelf Res.* 85, 42–59.
- Albuquerque, A.L.S., Belém, A.L., Zuluaga, F.J.B., Cordeiro, L.G.M., Mendoza, U., Knoppers, B.A., Gurgel, M.H.C., Meyers, P.A., Capilla, R., 2014. Particle Fluxes and Bulk Geochemical Characterization of the Cabo Frio Upwelling System in Southeastern Brazil: Sediment Trap experiments between spring 2010 and Summer 2012. *An. Acad. Bras. Cienc.* 86, 601–620. <https://doi.org/10.1590/0001-37652014107212>.
- Almeida, F.K., Mello, R.M., Costa, K.B., Toledo, F.A.L., 2015. The response of deep-water benthic foraminiferal assemblages to changes in paleoproductivity during the Pleistocene (last 769.2 kyr), western South Atlantic Ocean. *Palaeogeogr. Palaeoclimatol. Palaeoecol.* 440, 201–212.
- Al-Sabouni, N., Kucera, M., Schmidt, D.N., 2007. Vertical niche separation control of diversity and size disparity in planktonic foraminifera. *Mar. Micropaleontol.* 63 (1–2), 75–90.
- Arruda, W.Z., Campos, E.J.D., Zharkov, V., Soutelino, R.G., da Silveira, I.C.A., 2013. Events of equatorward translation of the Vitoria Eddy. *Cont. Shelf Res.* 70, 61–73.
- Barth, A.M., Clark, P.U., Bill, N.S., He, F., Pisias, N.G., 2018. Climate evolution across the Mid-Brunhes transition. *Clim. Past* 14 (12), 2071–2087.
- Bazin, L., et al., 2013. An optimized multi-proxy, multi-site Antarctic ice and gas orbital chronology (AICC2012): 120–800 ka. *Clim. Past* 9 (4), 1715–1731.
- Becquey, S., Gersonde, R., 2002. Past hydrographic and climatic changes in the Subantarctic Zone of the South Atlantic—the Pleistocene record from ODP Site 1090. *Palaeogeogr. Palaeoclimatol. Palaeoecol.* 182 (3), 221–239.
- Belem, A.L., Castelao, R.M., Albuquerque, A.L., 2013. Controls of subsurface temperature variability in a western boundary upwelling system. *Geophys. Res. Lett.* 40, 1362–1366. <https://doi.org/10.1002/grl.50297>.
- Berger, A., 1978. Long-term variations of daily insolation and quaternary climatic changes. *J. Atmos. Sci.* [https://doi.org/10.1175/1520-0469\(1978\)035<2362:LTVODI>2.0.CO;2](https://doi.org/10.1175/1520-0469(1978)035<2362:LTVODI>2.0.CO;2).
- Berger, A., Loutre, M.F., 1991. Insolation values for the climate of the last 10 million years. *Quat. Sci. Rev.* 10 (4), 297–317.
- Berger, W.H., Wefer, G., 2003. On the dynamics of the ice ages: stage-11 paradox, mid-brunhes climate shift, and 100-ky cycle. In: *Earth's Clim. Orbital Eccentricity. Mar. Isot. Stage 11 Quest. Geophys. Monogr.*, vol. 137. pp. 41–59. <https://doi.org/10.1029/137GM04>.
- Berger, A., Loutre, M.F., Mélice, J.L., 2006. Equatorial insolation: from precession harmonics to eccentricity frequencies. *Clim. Past Discuss.* 2, 519–533. <https://doi.org/10.5194/cpd-2-519-2006>.

- Berger, A., Loutre, M.F., Kaspar, F., Lorenz, S.J., 2007. 2. Insolation during interglacial. *Dev. Quat. Sci.* 7, 13–27. [https://doi.org/10.1016/S1571-0866\(07\)80027-3](https://doi.org/10.1016/S1571-0866(07)80027-3).
- Bolli, H.M., Saunders, J.B., 1985. Oligocene to Holocene low latitude planktic foraminifera. In: Bolli, H.M., Saunders, J.B., Perch-Nielsen, K. (Eds.), *Plankton Stratigraphy*. Cambridge Earth Science Series, vol. 1. Cambridge University, Cambridge, pp. 155–262.
- Calado, L., da Silveira, I.C.A., Gangopadhyay, A., de Castro, B.M., 2010. Eddy-induced upwelling off Cape São Tomé (22° S, Brazil). *Cont. Shelf Res.* 30, 1181–1188. <https://doi.org/10.1016/j.csr.2010.03.007>.
- Campos, E.J.D., Velhote, D., Da Silveira, I.C.A., 2000. Shelf break upwelling driven by Brazil current cyclonic meanders. *Geophys. Res. Lett.* 27, 751–754. <https://doi.org/10.1029/1999GL010502>.
- Campos, P.C., Möller, O.O., Piola, A.R., Palma, E.D., 2013. Seasonal variability and coastal upwelling near Cape Santa Marta (Brazil). *J. Geophys. Res. Oceans* 118 (3), 1420–1433.
- Candy, I., Mcclumont, E.L., 2013. Interglacial intensity in the North Atlantic over the last 800,000 years: investigating the complexity of the mid-Brunhes Event. *J. Quat. Sci.* 28, 343–348. <https://doi.org/10.1002/jqs.2632>.
- Candy, I., Schreve, D.C., Sherriff, J., Tye, G.J., 2014. Marine Isotope Stage 11: Palaeoclimates, palaeoenvironments and its role as an analogue for the current interglacial. *Earth-Science Rev.* 128, 18–51. <https://doi.org/10.1016/j.earscirev.2013.09.006>.
- Castelao, R.M., Barth, J.A., 2006. Upwelling around Cabo Frio, Brazil: the importance of wind stress curl. *Geophys. Res. Lett.* 33, 2–5. <https://doi.org/10.1029/2005GL025182>.
- Chalk, T.B., Hain, M.P., Foster, G.L., Rohling, E.J., Sexton, P.F., Badger, M.P.S., Cherry, S.G., Hasenfratz, A.P., Haug, G.H., Jaccard, S.L., AMartínez-García, A., Pälike, H., Pancost, R.D., Wilson, P.A., 2017. Causes of ice age intensification across the Mid-Pleistocene transition. *Proc. Natl. Acad. Sci.* 114 (50), 13114–13119.
- Coelho, C.A., De Oliveira, C.P., Ambrizzi, T., Reboita, M.S., Carpenedo, C.B., Campos, J.L.P.S., Tomaziello, A.C.N., Pampuch, R.A., Custódio, Mdutra, Livia, M.M., Da Rocha, R.P., Rehbein, A., 2016. The 2014 Southeast Brazil austral summer drought: regional scale mechanisms and teleconnections. *Clim. Dyn.* 46 (11–12), 3737–3752.
- Cruz, F.W., Burns, S.J., Karmann, I., Sharp, W.D., Vuille, M., 2006. Reconstruction of regional atmospheric circulation features during the late Pleistocene in subtropical Brazil from oxygen isotope composition of speleothems. *Earth Planet. Sci. Lett.* 248 (1–2), 495–507.
- Desprat, S., Sánchez Goñi, M.F., Naughton, F., Turon, J.L., Duprat, J., Malaizé, B., Cortijo, E., Peyrouquet, J.P., 2007. 25. Climate variability of the last five isotopic interglacials: Direct land-sea-ice correlation from the multiproxy analysis of North-Western Iberian margin deep-sea cores. *Dev. Quat. Sci.* 7, 375–386. [https://doi.org/10.1016/S1571-0866\(07\)80050-9](https://doi.org/10.1016/S1571-0866(07)80050-9).
- Droxler, A.W., Alley, R.B., Howard, W.R., Poore, R.Z., Burckle, L.H., Anonymous, 2003. Unique and exceptionally long interglacial marine isotope stage 11: window into Earth warm future climate. *Geophys. Monogr.* 137, 1–14. <https://doi.org/10.1029/137GM01>.
- Epica, C.M., 2004. Eight glacial cycles from an Antarctic ice core. *Nature* 429, 623–628.
- Fischer, N., Jungclauss, J.H., 2010. Effects of orbital forcing on atmosphere and ocean heat transports in Holocene and Eemian climate simulations with a comprehensive Earth system model. *Clim. Past* 6, 155–168. <https://doi.org/10.5194/cp-6-155-2010>.
- Gaeta, S.A., Lorenzetti, J.A., de Miranda, L.B., Susini-Ribeiro, S.M.M., Pompeu, M., De Araujo, C.E.S., 1999. The Vitória Eddy and its relation to the phytoplankton biomass and primary productivity during the austral fall of 1995. *Arch. Fishery Mar. Res.* 47 (2–3), 253–270.
- Ganopolski, A., Calov, R., 2011. The role of orbital forcing, carbon dioxide and regolith in 100 kyr glacial cycles. *Clim. Past* 7, 1415–1425. <https://doi.org/10.5194/cp-7-1415-2011>.
- Garreaud, R.D., Vuille, M., Compagnucci, R., Marengo, J., 2009. Present-day south American climate. *Palaeogeogr. Palaeoclimatol. Palaeoecol.* 281, 180–195. <https://doi.org/10.1016/j.palaeo.2007.10.032>.
- Giraudeau, J., Monteiro, P.M.S., Nikodemus, K., 1993. Distribution and malformation of living coccolithophores in the northern Benguela upwelling system off Namibia. *Mar. Micropaleontol.* 22 (1), 93–110.
- Hammer, Ø., Harper, D.A.T., Ryan, P.D., 2001. PAST: Paleontological statistics software package for education and data analysis. *Palaeontol. Electron.* 4, 1–9. <https://doi.org/10.1016/j.bcp.2008.05.025>.
- Hemleben, C., Spindler, M., Anderson, O.R., 1989. *Modern Planktonic Foraminifera*. Springer, Berlin, Heidelberg, New York (363 pp.).
- Hutson, W.H., 1980. The Agulhas current during the late Pleistocene: analysis of modern faunal analogs. *Science* 207 (4426), 64–66.
- Kim, J.-H., Schneider, R.R., Mulitza, S., Müller, P.J., 2003. Reconstruction of SE trade-wind intensity based on sea-surface temperature gradients in the Southeast Atlantic over the last 25 kyr. *Geophys. Res. Lett.* 30. <https://doi.org/10.1029/2003GL017557>.
- Kostadinov, T.S., Gilb, R., 2014. Earth Orbit v2. 1: a 3-D visualization and analysis model of Earth's orbit, Milankovitch cycles and insolation. *Geosci. Model Dev.* 7 (3), 1051–1068.
- Kucera, M., et al., 2005. Reconstruction of sea-surface temperatures from assemblages of planktonic foraminifera: multi-technique approach based on geographically constrained calibration data sets and its application to glacial Atlantic and Pacific Oceans. *Quat. Sci. Rev.* 24 (7–9), 951–998.
- Laepfle, T., Lohmann, G., 2009. Seasonal cycle as template for climate variability on astronomical timescales. *Paleoceanography* 24, 1–15. <https://doi.org/10.1029/2008PA001674>.
- Lessa, D.V., Ramos, R.P., Barbosa, C.F., da Silva, A.R., Belem, A., Turcq, B., Albuquerque, A.L., 2014. Planktonic foraminifera in the sediment of a western boundary upwelling system off Cabo Frio, Brazil. *Mar. Micropaleontol.* 106, 55–68. <https://doi.org/10.1016/j.marmicro.2013.12.003>.
- Lessa, D.V., Venancio, I.M., dos Santos, T.P., Belem, A.L., Turcq, B.J., Sifeddine, A., Albuquerque, A.L.S., 2016. Holocene oscillations of Southwest Atlantic shelf circulation based on planktonic foraminifera from an upwelling system (off Cabo Frio, Southeastern Brazil). *The Holocene* 26, 1175–1187. <https://doi.org/10.1177/0959683616638433>.
- Lessa, D.V.O., Santos, T.P., Venancio, I.M., Albuquerque, A.L.S., 2017. Offshore expansion of the Brazilian coastal upwelling zones during Marine Isotope Stage 5. *Glob. Planet. Chang.* 158, 13–20. <https://doi.org/10.1016/j.gloplacha.2017.09.006>.
- Lisiecki, L.E., Raymo, M.E., 2005. A Pliocene-Pleistocene stack of 57 globally distributed benthic $\delta^{18}\text{O}$ records. *Paleoceanography* 20, 1–17. <https://doi.org/10.1029/2004PA001071>.
- Matsuzaki, K.M.R., Eynaud, F., Malaizé, B., Grousset, F.E., Tisserand, A., Rossignol, L., Charlier, K., Jullien, E., 2011. Paleoclimatology of the Mauritanian margin during the last two climatic cycles: from planktonic foraminifera to African climate dynamics. *Mar. Micropaleontol.* 79, 67–79. <https://doi.org/10.1016/j.marmicro.2011.01.004>.
- Meckler, A.N., Clarkson, M.O., Cobb, K.M., Sodemann, H., Adkins, J.F., 2012. Interglacial Hydroclimate in the Tropical West Pacific through the late Pleistocene. *Science* 336 (6086), 1301–1304. <https://doi.org/10.1126/science.1218340>.
- Mohtadi, M., Hebbeln, D., Marchant, M., 2005. Upwelling and productivity along the Peru–Chile current derived from faunal and isotopic compositions of planktic foraminifera in surface sediments. *Mar. Geol.* 216 (3), 107–126.
- Mohtadi, M., et al., 2007. Modern environmental conditions recorded in surface sediment samples off W and SW Indonesia: planktonic foraminifera and biogenic compounds analyses. *Mar. Micropaleontol.* 65 (1–2), 96–112.
- Müller, U.C., Pross, J., 2007. Lesson from the past: present insolation minimum holds potential for glacial inception. *Quat. Sci. Rev.* 26, 3025–3029.
- Muller-Karger, F., Varela, R., Thunell, R., Scranton, M., Bohrer, R., Taylor, G., Capelo, J., Astor, Y., Tappa, E., Ho, T.-Y., Walsh, J.J., 2001. Annual cycle of primary production in the Cariaco Basin: Response to upwelling and implications for vertical export. *J. Geophys. Res. Ocean.* 106, 4527–4542. <https://doi.org/10.1029/1999JC000291>.
- PAGES, P.I.W.G. of P., 2016. Interglacials of the last 800,000 years. *Rev. Geophys.* 54, 162–219. <https://doi.org/10.1002/2015RG000482>.
- Patterson, R.T., Fishbein, E., 1989. Re-examination of the statistical methods used to determine the number of point counts needed for micropaleontological quantitative research. *J. Paleontol.* 63, 245–248. <https://doi.org/10.1017/S0022336000019272>.
- Peeters, F.J.C., Brummer, G.J., Ganssen, G., 2002. The effect of upwelling on the distribution and stable isotope composition of *Globigerina bulloides* and *Globigerinoides ruber* (planktic foraminifera) in modern surface waters of the NW Arabian Sea. *Glob. Planet. Chang.* 34, 269–291. [https://doi.org/10.1016/S0921-8181\(02\)00120-0](https://doi.org/10.1016/S0921-8181(02)00120-0).
- Peterson, R.G., Stramma, L., 1991. Upper-level circulation in the South-Atlantic Ocean. *Prog. Oceanogr.* 26, 1–73. [https://doi.org/10.1016/0079-6611\(91\)90006-8](https://doi.org/10.1016/0079-6611(91)90006-8).
- Petro, S.M., Pivel, M.A.G., Coimbra, J.C., Mizusaki, A.M.P., 2016. Paleoclimatographic changes through the last 130 ka in the Western South Atlantic based on planktonic foraminifera. *Revista Brasileira de Paleontologia* 19 (1), 3–14.
- Portilho-Ramos, R., Ferreira, F., Calado, L., Frontalini, F., de Toledo, M.B., 2015. Variability of the upwelling system in the southeastern Brazilian margin for the last 110,000 years. *Glob. Planet. Chang.* <https://doi.org/10.1016/j.gloplacha.2015.11.003>.
- Reboita, M.S., Ambrizzi, T., Silva, B., Pinheiro, R., Da Rocha, R.P., 2019. The South Atlantic subtropical anticyclone: present and future climate. *Front. Earth Sci.* 7, 8.
- Rodrigues, R.R., Lorenzetti, J.A., 2001. A numerical study of the effects of bottom topography and coastline geometry on the Southeast Brazilian coastal upwelling. *Cont. Shelf Res.* 21, 371–394. [https://doi.org/10.1016/S0278-4343\(00\)00094-7](https://doi.org/10.1016/S0278-4343(00)00094-7).
- Romero, O., Schmieder, F., 2006. Occurrence of thick *Ethmodiscus* oozes associated with a terminal Mid-Pleistocene transition event in the oligotrophic subtropical South Atlantic. *Palaeogeogr. Palaeoclimatol. Palaeoecol.* 235 (4), 321–329.
- Salgueiro, E., et al., 2008. Planktonic foraminifera from modern sediments reflect upwelling patterns off Iberia: insights from a regional transfer function. *Mar. Micropaleontol.* 66 (3), 135–164.
- Santos, T.P., et al., 2017. Prolonged warming of the Brazil current precedes deglaciations. *Earth Planet. Sci. Lett.* 463, 1–12.
- Schmid, C., Schäfer, H., Zenk, W., Podestá, G., 1995. The Vitória Eddy and its relation to the Brazil current. *J. Phys. Oceanogr.* 25 (11), 2532–2546.
- Schmieder, F., von Dobeneck, T., Bleil, U., 2000. The Mid-Pleistocene climate transition as documented in the deep South Atlantic Ocean: initiation, interim state and terminal event. *Earth Planet. Sci. Lett.* 179, 539–549.
- Schulz, M., Mudelsee, M., 2002. REDFIT: estimating red-noise spectra directly from unevenly spaced paleoclimatic time series. *Comput. Geosci.* 28, 421–426. [https://doi.org/10.1016/S0098-3004\(01\)00044-9](https://doi.org/10.1016/S0098-3004(01)00044-9).
- Silva, W.L., Nascimento, M.X., Menezes, W.F., 2015. Atmospheric blocking in the South Atlantic during the summer 2014: a synoptic analysis of the phenomenon. *Atmos. Climate Sci.* 5 (04), 386.
- Silveira, I.C.A. da, Schmidt, A.C.K., Campos, E.J.D., Godoi, S.S., Ikeda, Y., 2000. A corrente do Brasil ao largo da costa leste brasileira. *Rev. Bras. Oceanogr.* 48 (2), 171–183. <https://doi.org/10.1590/S1413-77392000000200008>.
- Souto, D.D., de Oliveira Lessa, D.V., Albuquerque, A.L.S., Sifeddine, A., Turcq, B.J., Barbosa, C.F., 2011. Marine sediments from southeastern Brazilian continental shelf: a 1200 year record of upwelling productivity. *Palaeogeogr. Palaeoclimatol. Palaeoecol.* 299, 49–55. <https://doi.org/10.1016/j.palaeo.2010.10.032>.
- Stramma, L., England, M., 1999. On the water masses and mean circulation of the South Atlantic Ocean. *J. Geophys. Res.* 104 (C9), 20863–20883.
- Sun, X., Cook, K.H., Vizy, E.K., 2017. The South Atlantic Subtropical High: Climatology

- and Interannual Variability. *J. Clim.* 30, 3279–3296. <https://doi.org/10.1175/JCLI-D-16-0705.1>.
- Thiede, J., 1975. Distribution of foraminifera in surface waters of a coastal upwelling area. *Nature* 253 (5494), 712–714.
- Toledo, F.A., Costa, K.B., Pivel, M.A., Campos, E.J., 2008. Tracing past circulation changes in the western South Atlantic based on planktonic foraminifera. *Revista Brasileira de Paleontologia* 11 (3), 169–178.
- Toledo, F.A.L., Quadros, J.P., Camillo, E., Santarosa, A.C.A., Flores, J.A., Costa, K.B., 2016. Plankton biochronology for the last 772,000??Years from the western South Atlantic Ocean. *Mar. Micropaleontol.* 127, 50–62. <https://doi.org/10.1016/j.marmicro.2016.07.002>.
- Valentin, J.L., 1984. Analyse des parametres hydrobiologiques dans la remontee de Cabo Frio (Bresil). vol. 276. pp. 259–276.
- Valentin, J.L., Andre, D.L., Jacob, S.A., 1987. Hydrobiology in the Cabo Frio (Brazil) upwelling: two-dimensional structure and variability during a wind cycle. *Cont. Shelf Res.* 7 (1), 77–88.
- Venancio, I.M., Belem, A.L., dos Santos, T.H.R., Zucchi, M. do R., Azevedo, A.E.G., Capilla, R., Albuquerque, A.L.S., 2014. Influence of continental shelf processes in the water mass balance and productivity from stable isotope data on the Southeastern Brazilian coast. *J. Mar. Syst.* 139, 241–247. <https://doi.org/10.1016/j.jmarsys.2014.06.009>.
- Venancio, I.M., Franco, D., Belem, A.L., MUltiza, S., Siccha, M., Albuquerque, A.L.S., Schulz, M., Kucera, M., 2016. Planktonic foraminifera shell fluxes from a weekly resolved sediment trap record in the southwestern Atlantic: evidence for synchronized reproduction. *Mar. Micropaleontol.* 125, 25–35.
- Venancio, I.M., Belem, A.L., Santos, T.P., Lessa, D.O., Albuquerque, A.L.S., MUltiza, S., Schulz, M., Kucera, M., 2017. Calcification depths of planktonic foraminifera from the southwestern Atlantic derived from oxygen isotope analyses of sediment trap material. *Mar. Micropaleontol.* 136, 37–50.
- Veres, D., et al., 2013. The Antarctic ice core chronology (AICC2012): an optimized multi-parameter and multi-site dating approach for the last 120 thousand years. *Clim. Past* 9 (4), 1733–1748.
- Weber, M.E., Wiedicke, M., Riech, V., Erlenkeuser, H., 1995. Carbonate preservation history in the Peru Basin: Paleooceanographic implications. *Paleoceanography* 10, 775–800. <https://doi.org/10.1029/95PA01566>.
- Yin, Q., 2013. Insolation-induced mid-Brunhes transition in Southern Ocean ventilation and deep-ocean temperature. *Nature* 494 (7436), 222–225.
- Yin, Q., Berger, A., 2015. Interglacial analogues of the Holocene and its natural near future. *Quat. Sci. Rev.* 120, 28–46. <https://doi.org/10.1016/j.quascirev.2015.04.008p>.